DFT-based *ab initio* study of structural and electronic properties of lithium fluorooxoborate LiB_6O_9F and experimentally observed second harmonic generation

B. Andriyevsky,[1,2,*] K. Doll,[1,3] G. Cakmak,[1] M. Jansen,[1] A. Niemer,[4] and K. Betzler[4]

[1]*Max Planck Institute for Solid State Research, Heisenbergstrasse 1, D-70569 Stuttgart, Germany*

[2]*Faculty of Electronics and Computer Sciences, Koszalin University of Technology, Śniadeckich Str. 2, PL-75-453 Koszalin, Poland*

[3]*Institute for Mathematical Physics, TU Braunschweig, Mendelssohnstr. 3, D-38106 Braunschweig, Germany*

[4]*Faculty of Physics, University of Osnabrück, Barbarastr. 7, D-49076 Osnabrück, Germany*

(Received 23 February 2011; revised manuscript received 1 July 2011; published 9 September 2011)

An *ab initio* density functional theory–based study of the electronic band structure, the elastic, electric, elastoelectric, and linear and nonlinear optical properties of the new ion conductor LiB_6O_9F, has been performed. The computed band structure reveals a wide direct band gap. The coefficients of the second order nonlinear susceptibility $\chi^{(2)}$ were found to be comparable to those of KH_2PO_4. Corresponding experimental investigations of second harmonic generation comply with the respective *ab initio* calculations.

DOI: 10.1103/PhysRevB.84.125112 PACS number(s): 71.20.Ps, 42.70.Mp, 42.65.Ky, 66.30.Dn

I. INTRODUCTION

Solid alkali ion conductors are constitutional components of all solid state electric batteries, and Li^+ ions comprising solid materials are among the top-performing conductors. A new material, LiB_6O_9F (LBOF), has recently been synthesized, and its crystal structure and electric conductivity have been studied.[1]

The fundamental prerequisites for high conductivity are well understood.[2] The anionic matrix needs to provide two dimensionally, or better three dimensionally, branched migration paths along which the ions experience a flat electrostatic potential profile. Researchers must avoid accumulations of negative charges on the walls of the pathways that might trap the moving cations, and LBOF was recently suggested as a candidate material.

LBOF crystallizes in space group $Pna2_1$. Figure 1 displays a view of the unit cell, which contains four formula units ($Z = 4$) and is characterized by the experimental parameters $a = 7.6555(1)$ Å, $b = 8.5318(1)$ Å, and $c = 10.7894(2)$ Å. The corresponding density of the crystal is equal to 2.213 g/cm^3.[1]

Because LBOF crystallizes in a noncentrosymmetric space group and consists of boroxine (B_3O_3) rings, its electronic structure and related properties can be expected to be similar to those of other boroxine rings containing crystals, e.g., LiB_3O_5 (lithium triborate or LBO),[3] $Li_2B_4O_7$,[4] and $CsLiB_6O_{10}$.[5] These materials are known to be good nonlinear optical materials used for different nonlinear optical applications. Therefore, the goal of the present work has been to measure and calculate the electronic structure and nonlinear optical properties of LBOF and to compare the results with the respective properties of LBO.

LBO is a biaxial crystal and has been proved to be an attractive material for pulsed optical parametric oscillators and amplifiers.[6] LBO has a short wavelength transmission limit of 160 nm, making it extremely suitable for applications in the ultraviolet (UV) spectrum. Because of the sensitive thermal dependence of its principal refractive indices,[7,8] it has wide temperature tunability, which is a rather beneficial feature. Although LBO has a moderate nonlinear coefficient (∼1 pm/V), it offers several major advantages: it has a wide transparency range (0.16 – 2.6 μm) and shows strong birefringence, which makes it applicable for the generation of radiation tunable from near UV to near infrared (IR); the surface-damage threshold of LBO is the highest of any nonlinear optical crystal measured so far.[3]

II. METHOD

In the present investigation, the first-principles code CRYSTAL[9] was used, which employs a local basis set. Full geometry optimization[10] was performed, and the energy vs. volume curves $E(V)$ were computed for various configurations. Subsequently, the polarization P, bulk modulus B, coefficients of the elastic stiffness c_{kl} ($k, l = 1, 2, \ldots, 6$), and coefficients of the elastoelectric tensor e_{ik} ($i = 1, 2, 3$) were calculated using the same approach as in earlier studies.[11,12] The coupled perturbed Kohn-Sham method (CPKS) was used to compute linear optical properties.[13] The calculations were done within the framework of the hybrid functional B3LYP for the exchange and correlation part of the Hamiltonian. The following basis sets for the constituent atoms of LBOF and KH_2PO_4 (KDP) were used: 6-11G for Li,[14] 6-21G* for B,[15] 8-411 for O,[16] 7-311G for F,[17] 86-511G for K,[18] 86-31G for P,[18] and 3-11G for H.[19] K-point nets with $4 \times 4 \times 4$ and $6 \times 6 \times 6$ sampling points were used.

Calculations of the electronic dielectric permittivity $\varepsilon(\omega)$ of LBOF were performed using the *ab initio* total-energy and molecular dynamics program known as the Vienna *ab initio* simulation package (VASP) developed at the Universität Wien.[19] The projector-augmented wave method with the local density approximation (LDA) and the Perdew-Burke-Ernzerhof (PBE) exchange and correlation functionals were used. A cutoff energy E_{cutoff} of 520 eV for the plane waves and 18 irreducible k-points were used for the results presented. In addition, for calibration purposes, different cutoff energies and k-point samplings were tested.

The components of the ion-clamped nonlinear dielectric susceptibility d_{ijk} of LBOF were calculated using the density functional theory (DFT)–based plane wave pseudopotential code ABINIT[20] (version 6.0.4). The LDA exchange–correlation functional[21] was used for the calculations. The core electrons of the constituent atoms of LBOF were handled using

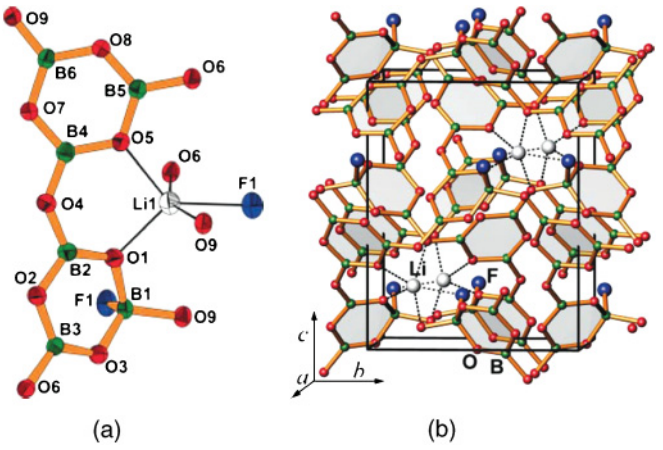

FIG. 1. (Color online) Repetition unit of the chainlike polyoxoanion (a) and crystal structure of LBOF with the margins of the unit cell (b). The B_3O_3 rings are emphasized in gray (Ref. 1).

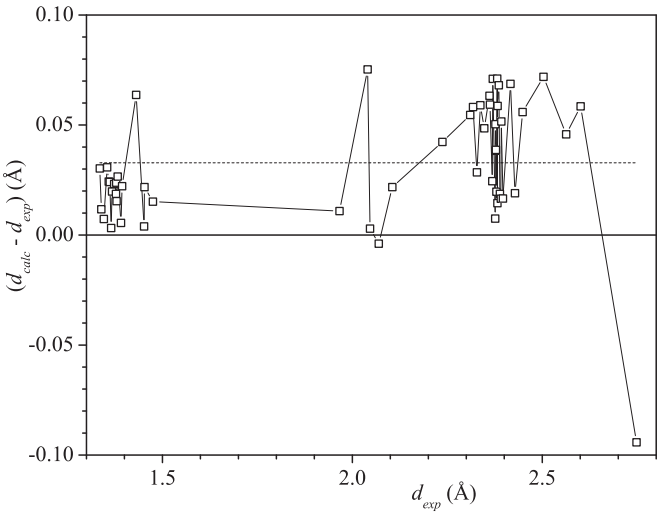

FIG. 2. Differences of calculated and experimental interatomic distances ($d_{\mathrm{calc}} - d_{\mathrm{exp}}$) of the atoms of the LBOF unit cell as a function of the experimental d_{exp} in the range from 1.3 to 2.8 Å. The dashed line is an averaged magnitude of ($d_{\mathrm{calc}} - d_{\mathrm{exp}}$). The standard deviation is SD = 0.027 Å.

nonlocal pseudopotentials of the Troullier-Martins type. The cutoff energy was chosen at 600 eV. Additional tests at different cutoff energies were performed. Six k-points in the irreducible part of the Brillouin zone were used. This corresponds to the default grid used by this code for the calculation of response functions for a unit cell of this size.

III. RESULTS AND DISCUSSION

A. Band structure and density of states of LBOF

The experimentally determined unit cell dimensions a, b, and c and the fractional coordinates[1] were used as the initial geometry for the DFT-based calculations using the CRYSTAL code. In view of the forthcoming calculations of the elastic constants, spontaneous polarization, piezoelectric constants, and optical properties, it was necessary to perform an optimization (relaxation) of the initial crystal structure. The optimized unit cell parameters and atomic positions were found to be close to those obtained from the experiment. Figure 2 illustrates deviations of the calculated and experimental interatomic distances. The standard deviation of a set of these differences is relatively small at SD = 0.027 Å. Similar results were obtained for the case of a larger atomic basis set.

The results of the Mulliken population analysis are displayed in Table I, with atom labels as in Fig. 1. The boron atoms carry a charge of +1.1 to +1.2, oxygen is negatively charged (from −0.7 to −1.0), fluorine has a charge of −0.5, and the lithium charge is +1.0. For comparison, in the case of LBO, the Mulliken charges are obtained as +1.2 (boron), −0.9 to −1.0 (oxygen), and +1.0 (lithium).

The band structure of LBOF, as obtained on the optimized crystal structure (with the B3LYP exchange–correlation functional), is displayed in Fig. 3(a). There is a relatively large direct (Γ-Γ) energy gap $E_g^{(\mathrm{B3LYP})} \approx 8.83$ eV, which means a wide photon energy range of optical transparency. The corresponding wavelength $\lambda = 140$ nm is in good agreement with the bottom boundary of the experimental transparency range (160–2600 nm) for the related compound LBO.[3] The direct character (Γ-Γ) of the gap makes the crystal suitable for laser light generation. The direct (Γ-Γ) energy gap calculated using the LDA functional was found to be considerably smaller, being $E_g^{(\mathrm{LDA})} \approx 6.47$ eV.

The band structure of LBOF calculated for the k-points sequence X-Γ-Z has revealed that in the direction Γ-Z ([000]-[001]/2) near the Γ-point, the electron effective mass calculated at the top of the valence band is equal to $m_v^{(\Gamma-Z)} = -3.45\, m_e$ and at the bottom of the conduction band, $m_c^{(\Gamma-Z)} = 2.27\, m_e$, respectively. In the direction Γ-X ([000]-[100]/2) near the Γ-point, the analogous absolute values are a bit higher, $m_v^{(\Gamma-X)} = -4.76\, m_e$ and $m_c^{(\Gamma-X)} = 2.5\, m_e$. Taking into account the relatively small density of LBOF ($\rho = 2.081$ g/cm^3), the electron effective masses obtained may be regarded as sufficiently small ones, which indicates a comparatively high degree of delocalization of the corresponding electronic states in the crystal.

TABLE I. Mulliken populations of LBOF.

Atom	Charge
Li	1.0
B1	1.1
B2	1.1
B3	1.2
B4	1.2
B5	1.1
B6	1.2
O1	−0.9
O2	−0.7
O3	−0.8
O4	−0.9
O5	−0.8
O6	−0.9
O7	−0.7
O8	−0.7
O9	−1.0
F	−0.5

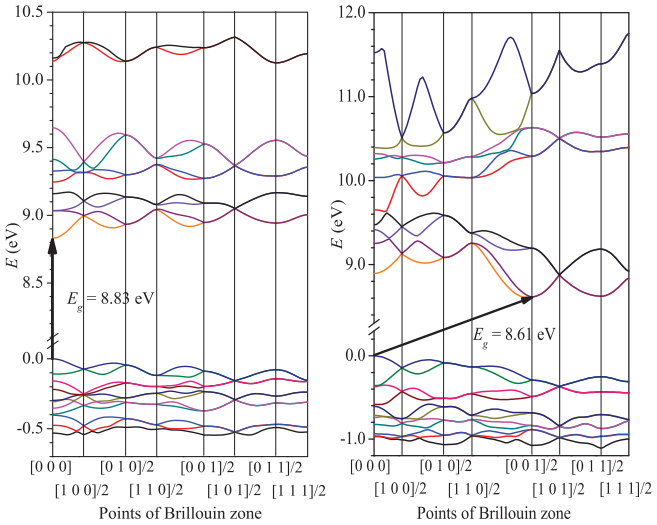

FIG. 3. (Color online) Electronic band structure of LBOF, $\rho = 2.1$ g/cm^3 (a), and of LBO, $\rho = 2.38$ g/cm^3 (b), for the optimized crystal structures, on the level of B3LYP.

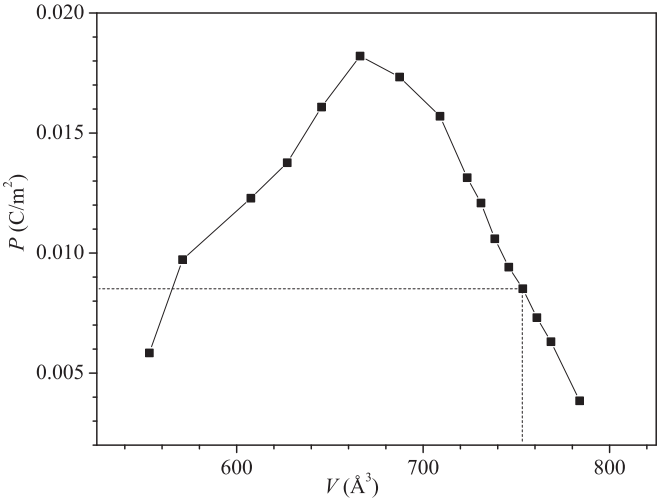

FIG. 4. Unit cell volume dependence of the absolute value of the polarization $P(V)$ of LBOF. The dashed line marks the computed equilibrium geometry.

LBO is known as a nonlinear optical material with relatively promising parameters, and it crystallizes in space group $Pna2_1$. The band structure of LBO [Fig. 3(b)] is substantially different from that of LBOF [Fig. 3(a)]: LBO has an indirect gap, and the band widths are smaller for LBO than for LBOF (at the level of the B3LYP functional). This is different from earlier calculations in which a direct gap was obtained[22–24]; see also the review in Ref. 25.

B. Elastic properties of LBOF

For the optimized crystal structure of LBOF, the coefficients of the elastic stiffness tensor c_{ij} $(i, j = 1, 2, \ldots, 6)$,

$$\sigma_i = \sum_j c_{ij}\varepsilon_j, \tag{1}$$

and the bulk modulus B,

$$B = -V\frac{\partial P}{\partial V} = V\frac{\partial^2 E}{\partial V^2}, \tag{2}$$

were calculated using the approach presented in Ref. 26. For the calculation of one coefficient of the elastic stiffness tensor c_{ij} or bulk modulus B, seven distortions in the range from -3% to 3% were applied. The values of B and c_{ij} as calculated are shown in Table II.

The bulk modulus B_v obtained on the basis of the calculated components c_{ij} agrees satisfactorily with the magnitude of the bulk modulus B:

$$B_v = [(c_{11} + c_{22} + c_{33}) + 2 \cdot (c_{12} + c_{13} + c_{23})]/9. \tag{3}$$

The components c_{ij} of the elastic stiffness tensor of LBOF were calculated for the clamped and nonclamped crystals. As expected, the c_{ij} values for the nonclamped crystal are smaller than those for the clamped one, and the corresponding relative differences reach 50% in the cases of c_{11} and c_{33}. The c_{22} value is the greatest, which agrees qualitatively with the spatial arrangement of the boron rings in the crystal structure: we can expect a smaller elastic compliance and higher elastic stiffness for the directions lying approximately in the plane of the boron rings.

C. Electric polarization and elastoelectric properties of LBOF

The electric polarization P of LBOF was calculated on the basis of the Berry phase approach[26,27] for different crystal unit cell volumes V. According to this approach, the polarization P of a crystal is the sum of the electronic P_{el} and ionic P_{ion} components,[28]

$$\vec{P} = \int dt \frac{1}{V_{\text{cell}}} \int_{\text{cell}} d\vec{r}\,\vec{j}(\vec{r},t) = \vec{P}_{\text{el}} + \vec{P}_{\text{ion}}. \tag{4}$$

The dependence of the polarization upon the unit cell volume $P(V)$ was analyzed (Fig. 4). At the equilibrium unit cell volume $V = 753.4$ Å^3, corresponding to the optimized crystal structure of LBOF, the polarization is equal to $P = -8.2\times10^{-3}$ C/m^2. The absolute value of the polarization P increases with decreasing unit cell volume V and achieves its maximum at 670 Å^3. Here, the value of polarization is twice as large as the one at the equilibrium volume (Fig. 4).

TABLE II. Bulk modulus B, elastic stiffness constants c_{ij}, and derivative bulk modulus B_v of LBOF in space group $Pna2_1$ (in 10^9 N/m^2).

Crystal	B	B_v	c_{11}	c_{22}	c_{33}	c_{12}	c_{13}	c_{23}	c_{44}	c_{55}	c_{66}
Clamped	26.9	29.9	40.8	108.8	38.2	−3.5	23.2	21.0	24.6	36.6	22.8
Nonclamped	27.2		24.1	89.5	20.0	−8.9					

TABLE III. Elastoelectric constants e_{ik} of LBOF (in 10^{-3} C/m^2).

	e_{31}	e_{32}	e_{33}	e_{24}	e_{15}
Clamped crystal	57	101	165	166	167
Nonclamped crystal	−39.4	−18.5	171	—	—

Because the derivative of the polarization with respect to the unit cell volume dP/dV at the equilibrium volume $V = 753.4$ Å^3 (Fig. 4) has a large value, the pyroelectric coefficient dP/dT in LBOF is also expected to be large, so there may be a practical interest for the use of LBOF as the active part of the detectors of IR radiation. If we estimate the thermal expansion of LBOF as being equal to $dV/V/dT = 10^{-5}$ K^{-1} (a typical order of magnitude for similar solids), then, taking into consideration the data in Fig. 4, the pyroelectric coefficient of LBOF will be on the order of $\gamma = dP/dT = 10^{-6}$ C/m^2/K. This is ∼30 times smaller than for triglycine sulfate at room temperature (0.32×10^{-4} C/m^2/K),[29] which is widely used as a good pyroelectric material.

The coefficients of the elastoelectric tensor e_{ki} of LBOF were calculated using the approach described in Ref. 9,

$$e_{ki} = \frac{|e|}{2\pi V}\sum_l a_{kl}\frac{d\varphi_l}{d\varepsilon_i}, \quad k, l = 1,2,3; \quad i = 1,2,...,6, \quad (5)$$

where V and a_{kl} are, respectively, the undistorted unit cell volume and component along the Cartesian axis k of the direct lattice vector $\boldsymbol{a_l}$. According to Eq. (5), the elastoelectric constants can be obtained by evaluating the phase φ as a function of the deformation of the unit cell parameters. The corresponding results for LBOF are presented in Table III.

The results obtained reveal significant differences between the elastoelectric constants calculated for the clamped and those calculated for the nonclamped crystals. For the clamped crystal, all elastoelectric constants e_{ik} are positive. Taking into account a negative magnitude of the polarization of nonstrained LBOF, this means that an elongation of the crystal in the orthogonal unit cell directions a, b, and c leads to the decrease of the absolute value of the spontaneous polarization. This conclusion agrees qualitatively with the results of the unit cell volume dependence of the polarization (Fig. 4). For the nonclamped crystal, however, two of the elastoelectric constants (e_{31} and e_{32}) are negative but relatively small (Table III).

D. Linear and nonlinear optical properties of LBOF and related materials

In view of the interest in boron-containing noncentrosymmetric crystals possessing good nonlinear optical characteristics,[3 30–32] we have calculated various optical properties. This was done to include several reference materials: LBO, KDP_*Fdd*2 (ferroelectric KH_2PO_4, space group *Fdd*2), and KDP_$I\bar{4}2d$ (paraelectric KH_2PO_4, space group $I\bar{4}2d$). LBO has a somewhat similar chemical composition to that of LBOF, possesses the same space group, and has been well studied because of its wide applications as a nonlinear optical material.[33,34] KDP_*Fdd*2 displays the same point group of symmetry *mm*2 (and therefore the same set of nonzero components of the tensors $\chi^{(2)}_{ijk}$ and $\chi^{(3)}_{ijkl}$). KDP_$I\bar{4}2d$ shows the point group symmetry $\bar{4}2d$. KDP was also chosen for our comparative study because its nonlinear optical properties were studied comprehensively in Ref. 18 and it is often used as a reference material for second harmonic generation (SHG).

In Table IV, the following calculated linear optical properties of LBOF, LBO, and KDP_*Fdd*2 are displayed, as obtained with various methods: the refractive index $n = \varepsilon^{1/2} = (\chi^{(1)} + 1)^{1/2}$, the birefringence Δn, the acute angle between the optical axes $2V$, and the optical sign.[35] The angle V was calculated using

$$\cos V = \frac{\alpha}{\beta}\sqrt{\frac{\gamma^2-\beta^2}{\gamma^2-\alpha^2}}, \quad (6)$$

where α, β, and γ are the principal refractive indices and $\alpha < \beta < \gamma$. The calculated values were obtained at the optimized unit cell dimensions and fractional atomic coordinates.

The computed values of the refractive indices agree reasonably well. We observe that the density functional with the largest gap gives the smallest value of the refractive indices, which is to be expected (see, e.g., Ref. 39). This trend can be seen when comparing the results for LDA, PBE, and B3LYP in Table IV: the LDA gap is smallest, and the refractive index is largest. The PBE gap is a bit larger, and the refractive index a bit smaller. Finally, the B3LYP gap is largest, and the refractive indices are smallest. However, the computed equilibrium volume is different for the various functionals. These different equilibrium volumes, depending on the functional, may indeed affect the computed refraction indices. According to the Lorentz-Lorenz (or Clausius-Mossotti) equation, the dielectric function depends on the density: $\frac{\varepsilon-1}{\varepsilon+2} = K\rho$. This relation does not hold for the present orthorhombic crystal type, and the polarizability that enters K also depends on the volume. Still, it may serve as an estimate. Indeed, when we compute the ratio of the computed equilibrium volumes of LBOF, on the LDA and PBE level, we obtain a ratio of $\rho^{(\mathrm{LDA})}/\rho^{(\mathrm{PBE})} = 1.11$. The corresponding ratio of $\frac{\varepsilon-1}{\varepsilon+2}^{(\mathrm{LDA})}/\frac{\varepsilon-1}{\varepsilon+2}^{(\mathrm{PBE})} \approx 1.08$ for the various $\varepsilon_x(\hbar\omega = 0)$, $\varepsilon_y(\hbar\omega = 0)$, $\varepsilon_z(\hbar\omega = 0)$ is close to the previously mentioned ratio of the densities.

The maximal birefringence, however, is higher for LBOF, $|\Delta n_{12}| \approx 0.08$, in comparison to LBO, $|\Delta n_{12}| \approx 0.06$, which indicates a larger optical anisotropy, corresponding to a greater anisotropy of the corresponding electronic system of LBOF.

Two other characteristics of optically biaxial crystals, the sign (+ or −) and the acute angle between the optical axes ($2V$), are important when analyzing optical anisotropies.[35]

In addition, the real and imaginary parts of the complex dielectric permittivity $\varepsilon(\hbar\omega)$ were computed for LBOF (Fig. 5). The figure presented is obtained with a cutoff energy of 520 eV and 18 irreducible K-points. Tests with fewer (8) and more (100) irreducible K-points, as well as tests with a lower (500 eV) and higher (600 eV) cutoff energy gave similar results, with deviations of the order of a few percent.

Having determined the dependences $\varepsilon_2(\hbar\omega)$ for the three principal directions of the optical indicatrix, we can estimate the possibility of SHG. It is seen from Fig. 5 that SHG in LBOF is expected to occur, because the same magnitude of the refractive indices $n_x = n_z$ is found for the reference and double frequencies ω, e.g., for $\hbar\omega = 1.85$ eV and $2\hbar\omega = 3.70$ eV.

TABLE IV. Calculated refractive indices n_i, birefringences Δn_{jk}, optical sign, and acute angle $2V$ between the optical axes of LBOF, LBO, and KDP_*Fdd*2 for the principal directions of the optical indicatrix 1 ≡ [100], 2 ≡ [010], and 3 ≡ [001]. $\hbar\omega$ corresponds to the photon energy, V_c to the computed equilibrium volume, E_g to the gap.

Parameter Compound Method Parameters	n_1	n_2	n_3	$\lvert\Delta n_{12}\rvert$	$\lvert\Delta n_{13}\rvert$	$\lvert\Delta n_{23}\rvert$	Sign $2V$ (degree)
LBOF CRYSTAL, B3LYP, CPKS $\hbar\omega = 0$, $V_c = 753.4$ Å^3, $E_g = 8.83$ eV	1.397	1.484	1.424	0.087	0.027	0.060	+ 69
LBOF VASP, LDA, $\hbar\omega = 0$, $E_{\text{cutoff}} = 525$ eV $V_c = 676.47$ Å^3, $E_g = 6.22$ eV	1.510	1.591	1.550	0.081	0.040	0.041	+ 46
LBOF VASP, PBE, $\hbar\omega = 0$, $E_{\text{cutoff}} = 520$ eV $V_c = 750.09$ Å^3, $E_g = 6.50$ eV	1.468	1.547	1.494	0.079	0.026	0.053	+ 72
LBO CRYSTAL, B3LYP, CPKS, $\hbar\omega = 0$, $V_c = 334.4$ Å^3, $E_g = 8.61$ eV	1.476	1.539	1.520	0.063	0.044	0.019	− 64
LBO VASP, PBE, $\hbar\omega = 0$, $E_{\text{cutoff}} = 400$ eV, $V_c = 316.83$ Å^3, $E_g = 6.45$ eV	1.629	1.689	1.652	0.060	0.023	0.037	+ 77
LBO (experiment)[30] $\hbar\omega = 1.5$ eV $E_g \approx 8.0$ eV[3]	1.569	1.610	1.595	0.041	0.026	0.015	− 73
KDP_*Fdd*2 VASP, PBE, $\hbar\omega = 0$, $E_{\text{cutoff}} = 400$ eV, $V_c = 822.79$ Å^3, $E_g = 5.40$ eV	1.512	1.484	1.447	0.028	0.065	0.037	− 80
KDP_*Fdd*2 CRYSTAL, B3LYP, CPKS, $\hbar\omega = 0$, $V_c = 816.90$ Å^3, $E_g = 7.82$ eV	1.422	1.405	1.364	0.017	0.058	0.041	− 63
KDP_*Fdd*2 (experiment)[36,37] $\hbar\omega = 2.105$ eV $E_g > 7.6$ eV[38]	1.516	1.504	1.470	0.012	0.046	0.034	— 61

Another precondition for SHG is a comparatively high second order nonlinear electronic susceptibility $\chi^{(2)}$,[40] which can be evaluated using the electric field dependence of the dielectric susceptibility $\chi(F) = \varepsilon(F) - 1$,[41]

$$\chi_{ij}(F) = \chi_{ij}^{(1)} + \chi_{ijk}^{(2)} F_k + \chi_{ijkl}^{(3)} F_k F_l + \chi_{ijklr}^{(4)} F_k F_l F_r + \cdots, \tag{7}$$

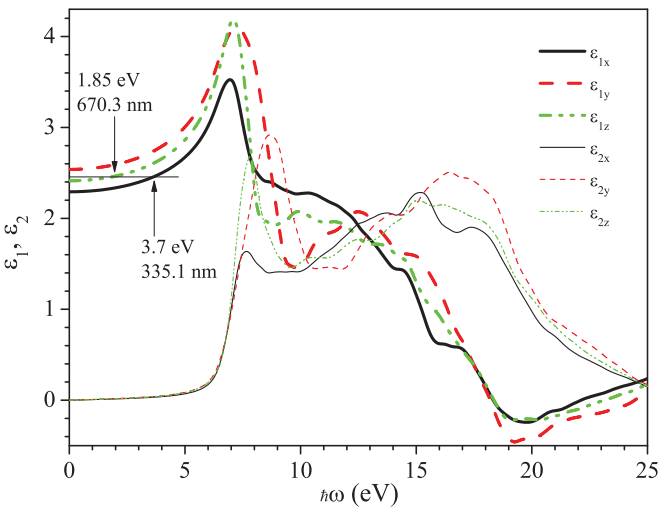

FIG. 5. (Color online) Spectra of real (ε_1) and imaginary (ε_2) parts of the dielectric permittivity $\varepsilon(\hbar\omega)$ of LBOF for light polarizations along the principal directions X, Y, and Z of the optical indicatrix, obtained using the VASP code, with LDA.

where $i, j, k, l, r = 1, 2, 3$. The tensor $\chi_{ij}^{(1)}$ has three principal components, $\chi_{11}^{(1)}$, $\chi_{22}^{(1)}$, and $\chi_{33}^{(1)}$, corresponding to the three principal refractive indices.[35] In the crystals with inversion symmetry or along the nonpolar directions, in the case of polar crystals, the susceptibility χ does not change when inverting the electric field; therefore, the even-order susceptibilities $\chi^{(2)}$, $\chi^{(4)}$, . . . are equal to zero in these cases. Some components of the tensors, $\chi_{ijk}^{(2)}$, $\chi_{ijkl}^{(3)}$, and $\chi_{ijklr}^{(4)}$, may be equal to zero due to symmetry conditions.[42]

For calculating all nonvanishing components of the second order susceptibility tensor $\chi_{ijk}^{(2)}$ of LBOF, LBO, KDP_*Fdd*2, and KDP_$I\bar{4}2d$, we used the ABINIT code.[20] This code employs perturbation theory within the framework of the independent particle picture.[43] Quasiparticle effects are neglected, which may be important due to their influence on the band gap, and have been suggested to be treated with, e.g., the scissor operator approach, the GW (where the self energy is approximated as the product of a Green function G and a screened interaction W) approximation,[44] or possibly hybrid functionals.[39] The corresponding results are gathered in Table V. The calculations refer to the static limit, whereas the experiments (see Sec. III F) are performed at a wavelength of $\lambda = 1064$ nm ($\hbar\omega = 1.165$ eV), in the present case. From Fig. 5, we can see that the linear optical response function shows a relatively small dispersion in this range. In the case of LBO,[45] we can similarly see that the second order susceptibility has only a small dispersion in the photon energy range of 0–4 eV.

TABLE V. Components of the linear susceptibility tensor $\chi^{(1)}_{ij}$ and independent components of the second order susceptibility tensor d_{ijk} (in 10^{-12} mV^{-1}) for LBOF, LBO, KDP_*Fdd*2, and KDP_$I\bar{4}2d$. The calculated values $\chi^{(1)}_{ij}$ and d_{ijk} were obtained using ABINIT code, with the LDA.

Crystal Parameter	LBOF	LBO	KDP_*Fdd*2	KDP_$I\bar{4}2d$
$\chi^{(1)}_{11}$/calc.	1.334	1.579	1.460	1.471
$\chi^{(1)}_{11}$/exp.	—	1.4614[30] ($\hbar\omega = 1.5$ eV)	1.2989[36,37] ($\hbar\omega = 2.105$ eV)	1.2473[30] ($\hbar\omega = 1.4$ eV)
$\chi^{(1)}_{22}$/calc.	1.540	1.737	1.450	1.471
$\chi^{(1)}_{22}$/exp.	—	1.5933[30] ($\hbar\omega = 1.5$ eV)	1.2614[36,37] ($\hbar\omega = 2.105$ eV)	1.2473[30] ($\hbar\omega = 1.4$ eV)
$\chi^{(1)}_{33}$/calc.	1.385	1.689	1.175	1.204
$\chi^{(1)}_{33}$/exp.	—	1.5454[30] ($\hbar\omega = 1.5$ eV)	1.1609[36,37] ($\hbar\omega = 2.105$ eV)	1.1359[30] ($\hbar\omega = 1.4$ eV)
d_{311}/calc.	0.029	−0.817	−0.427	—
d_{311}/exp.	—	−0.67[46]	0.8[46]	
d_{322}/calc.	0.255	1.092	0.463	—
d_{322}/exp.	—	0.85[46]	0.5[46]	
d_{333}/calc.	−0.235	−0.093	0.022	—
d_{333}/exp.	—	0.04[42]	<0.02[42]	
d_{123}/calc.	—	—	—	0.458
d_{123}/exp.	—	—	—	0.39[46]

Therefore, the static limit of values ($\hbar\omega = 0$) should be a sufficiently good approximation.

Concerning the accuracy, we performed test calculations on the simpler system LBO. We find that varying the cutoff energy between 490 and 760 eV changes the computed values of the second order susceptibilities in a range of ∼10%. For $d_{113} = d_{131} = d_{311}$, we obtain values between −0.800 and −0.850 (experiment: −0.67[46]); for $d_{223} = d_{232} = d_{322}$, values are between 1.09 and 1.25 (experiment: 0.85[46]); and for d_{333} values, are between −0.081 and −0.141 (experiment: 0.04[46]).

Therefore, LBOF appears to be a promising candidate for nonlinear optical conversion, including SHG. However, we must take into account that the efficiency of SHG depends on the whole set of nonvanishing components of the tensor $\chi^{(2)}_{ijk}$ (in the case of LBOF: $\chi^{(2)}_{113} = \chi^{(2)}_{131} = \chi^{(2)}_{311}$ and $\chi^{(2)}_{223} = \chi^{(2)}_{232} = \chi^{(2)}_{322}$ and $\chi^{(2)}_{333}$).[41,42]

E. Phase matching related to SHG in LBOF

For a principal realization of SHG in a crystal, the known phase matching conditions PM1 and/or PM2 have to be satisfied, in addition to the sufficiently high coefficients of the nonlinear dielectric susceptibility, $d_{ijk} = (\frac{1}{2})\chi^{(2)}_{ijk}$.[30] These phase matching conditions are derived from the principle of momentum conservation in a three photon process.[30] The phase matching condition PM1 leads to the relation

$$n||(2\hbar w) = n\perp(\hbar\omega), \tag{8}$$

where $n\|(2\hbar\omega)$ and $n\perp(\hbar\omega)$ are refractive indices in the spectral range of crystal transparency for two orthogonal polarizations of the light electric field, $F_\|$ and $F_\perp$, respectively. The phase matching condition PM2 concerns the interaction of two orthogonal light polarizations.[30] The photon energy dependencies of refractive indices $n_1(\hbar\omega)$, $n_2(\hbar\omega)$, and $n_3(\hbar\omega)$ give the possibility of checking the phase matching conditions PM1 and/or PM2, both of which are necessary for SHG. If these conditions are satisfied, then the efficiency of SHG will be directly proportional to the square of the respective effective coefficients of the nonlinear dielectric susceptibility d_{eff}. The susceptibility d_{eff} is a linear combination of all components of the tensor d_{ijk} ($i, j, k = 1, 2, 3$). The coefficients of this linear combination depend on the direction of light propagation, satisfying the phase matching conditions.[31,40,47]

For the study of the phase matching conditions in LBOF, we performed DFT-based *ab initio* calculations of the band structure and of the real and imaginary parts $\varepsilon_1(\hbar\omega)$ and $\varepsilon_2(\hbar\omega)$ of the dielectric function $\varepsilon(\hbar\omega)$ using the VASP code.[19] The corresponding results for the photon energy dependences of the refractive indices $n_i(\hbar\omega)$ ($i = a, b, c$) are presented in Fig. 6, together with the analogous results for LBO. The results obtained for the imaginary part of the dielectric function $\varepsilon_2(\hbar\omega)$ reveal a similar range of transparency for LBOF and LBO, $\hbar\omega < 7$ eV.

On the basis of the photon energy dependences of the refractive indices $n_i(\hbar\omega)$ obtained for LBOF, we have calculated the ranges of the angles Φ and Θ satisfying the phase matching conditions PM1 and PM2 by using the respective relations for biaxial crystals.[47] The range of the fundamental photon energy $\hbar\omega$ of SHG and the corresponding energy $\hbar\omega$ has been obtained to be 0.7–2.3 eV. The corresponding results for the photon energy $\hbar\omega = 1.165$ eV ($\lambda = 1064$ nm) are presented in Fig. 7. The maximal angular ranges of phase matching in LBOF were found to be for the energy $\hbar\omega = 1.4$ eV.

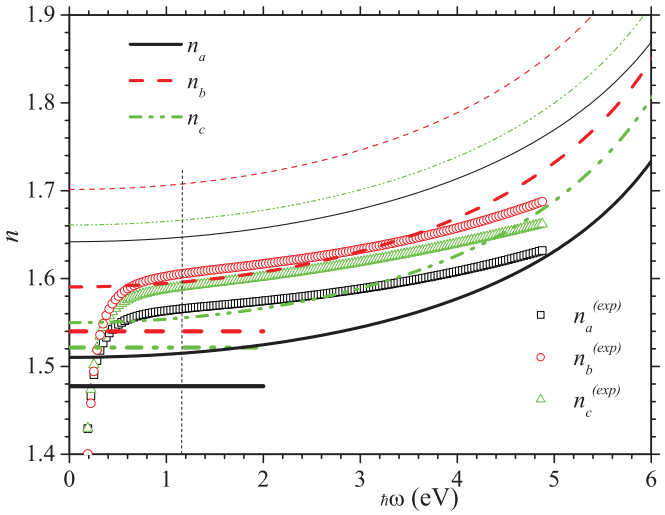

FIG. 6. (Color online) Photon energy dependences of the refractive indices $n_a(\hbar\omega)$, $n_b(\hbar\omega)$, and $n_c(\hbar\omega)$: LBOF computed with VASP (LDA) is indicated by thick lines in the range of 0–6 eV, LBO computed with VASP (LDA) is indicated by thin lines in the range of 0–6 eV, LBO computed with CRYSTAL (B3LYP, only for $\hbar\omega = 0$) is indicated by horizontal lines, and experimental LBO (Ref. 3) is indicated by squares (n_a), circles (n_b), and triangles (n_c). n_a, n_b, and n_c are refractive indices for the directions of the light polarization along the unit cell edges a, b, and c.

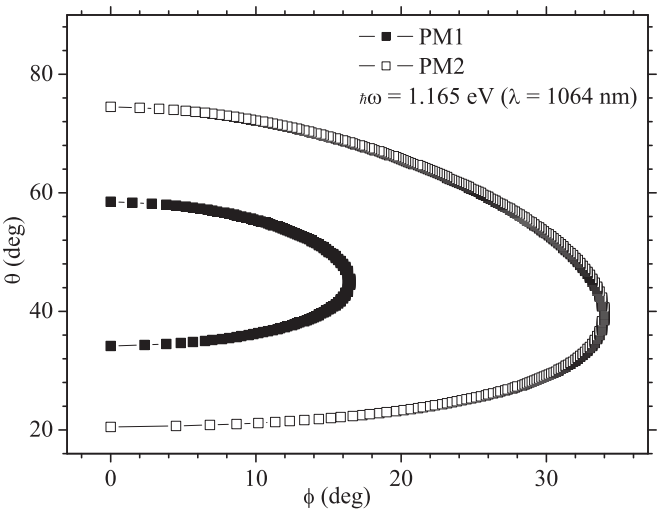

FIG. 7. Phase matching angles of LBOF (LDA) for type I (PM1) and type II (PM2) for the first photon energy $\hbar\omega = 1.165$ eV ($\lambda = 1064$ nm), plotted on the first quadrant.

There is a very sensitive dependence of the phase matching angle on the refractive indices[47]; consequently, as the different functionals give different refractive indices, the dependence on the functional is also very strong.

F. Experimental verification of SHG in LBOF

To verify SHG in LBOF experimentally, the corresponding measurements were performed using the SHG powder technique.[48] Samples of different size fractions were excited by a pulsed Nd:YAG laser with a fundamental wavelength of 1064 nm corresponding to a photon energy of 1.165 eV. We applied 40 μJ pulses with a repetition rate of ~20 Hz. The generated SHG light was collected by an integrating sphere and detected using a photomultiplier system with appropriate pulse processing electronics. Fundamental light was suppressed by an optical band-pass filter; second harmonic light was identified by a set of optical edge filters. As standards, KDP samples of identical geometry were chosen. The main results of the powder measurements include the following:

(1) The fraction size dependence proves that LBOF indeed shows phase matched SHG at a fundamental wavelength of 1064 nm.

(2) The intensity comparison with KDP reveals that the effective tensor element d_{eff} is slightly larger than that of KDP, $d_{\text{eff}}^{LBOF} \approx 1.4 d_{\text{eff}}^{KDP}$.

IV. CONCLUSIONS

The structural and electronic properties of LBOF were computed from first principles. LBOF was found to have a wide direct gap. Its bulk modulus is 30 GPa. It is ferroelectric, with the magnitude of the polarization being 8.2×10^{-3} C/m^2. A special emphasis was put on the nonlinear properties. The second order susceptibilities $\chi^{(2)}_{311}$ and $\chi^{(2)}_{322}$ of LBOF are smaller than the corresponding ones of LBO and KDP; $\chi^{(2)}_{333}$ was found to be larger. Calculations of the optical dielectric function and the phase matching conditions PM1 and PM2 reveal the possibility of SHG in LBOF for the first photon energy $\hbar\omega$ in the range of $\hbar\omega = 0.7$–2.3 eV. SHG was experimentally observed with a Nd:YAG laser, which complies with the calculations. Thus, LBOF promises to be a perspective candidate for nonlinear optical conversion.

ACKNOWLEDGMENTS

Some calculations were performed in the Wrocław Centre for Networking and Supercomputing of Wrocław University of Technology.

*bohdan.andriyevskyy@tu.koszalin.pl

[1] G. Cakmak, J. Nuss, and M. Jansen, Z. Anorg. Chem. **635**, 631 (2009).

[2] M. Jansen, Angew. Chem. Int. Ed. **30**, 1547 (1991).

[3] C. Chen, Y. Wu, A. Jiang, B. Wu, G. You, R. Li, and S. Lin, J. Opt. Soc. Am. B **6**, 616 (1989).

[4] M. M. Islam, V. V. Maslyuk, T. Bredow, and C. Minot, J. Phys. Chem. B **109**, 13597 (2005).

[5] Y. Mori, I. Kuroda, S. Nakajima, T. Sasaki, and S. Nakai, Appl. Phys. Lett. **67**, 1818 (1995).

[6] T. Schröder, K.-J. Boller, A. Fix, and R. Wallenstein, Appl. Phys. B **58**, 425 (1994).

[7]S. P. Velsko, M. Webb, L. Davis, and C. Huang, IEEE J. Quantum Electron. **27**, 2182 (1991).
[8]Y. Tang, Y. Cui, and M. H. Dunn, J. Opt. Soc. Am. B **12**, 638 (1995).
[9]R. Dovesi, V. R. Saunders, C. Roetti, R. Orlando, C. M. Zicovich-Wilson, F. Pascale, B. Civalleri, K. Doll, N. M. Harrison, I. J. Bush, Ph. D'Arco, M. Llunell, *User's Manual of CRYSTAL '09* (Torino, Italy, 2009).
[10]K. Doll, V. R. Saunders, N. M. Harrison, Int. J. Quant. Chem. **82**, 1 (2001); K. Doll, R. Dovesi, R. Orlando, Theor. Chem. Acc. **112**, 394 (2004); B. Civalleri, P. D'Arco, R. Orlando, V. R. Saunders, R. Dovesi, Chem. Phys. Lett. **348**, 131 (2001).
[11]B. Andriyevsky and K. Doll, J. Phys. Chem. Solids **70**, 84 (2009).
[12]B. Andriyevsky, K. Doll, and M. Jansen, J. Phys. Chem. Solids **71**, 357 (2010).
[13]M. Ferrero, M. Rerat, R. Orlando, and R. Dovesi, J. Chem. Phys. **128**, 014110 (2008).
[14]L. Ojamae, K. Hermansson, C. Pisani, M. Causà, and C. Roetti, Acta Cryst. B **50**, 268 (1994).
[15]R. Orlando, R. Dovesi, and C. Roetti, J. Phys. Condens. Matter **2**, 7769 (1990).
[16]M. D. Towler, N. L. Allan, N. M. Harrison, V. R. Saunders, W. C. Mackrodt, and E. Aprà, Phys. Rev. B **50**, 5041 (1994).
[17]R. Nada, C. R. A. Catlow, C. Pisani, and R. Orlando, Mater. Sci. Eng. **1**, 165 (1993).
[18]V. Lacivita, M. Rérat, B. Kirtman, M. Ferrero, R. Orlando, and R. Dovesi, J. Chem. Phys. **131**, 204509 (2009).
[19]G. Kresse and D. Joubert, Phys. Rev. **59**, 1758 (1999); *the guide of VASP*, [https://cms.mpi.univie.ac.at/marsweb/index.php].
[20]M. Veithen, X. Gonze, and Ph. Ghosez, Phys. Rev. B **71**, 125107 (2005); [http://www.abinit.org].
[21]J. P. Perdew and A. Zunger, Phys. Rev. B **23**, 5048 (1981).
[22]Y.-N. Xu and W. Y. Ching, Phys. Rev. B **41**, 5471 (1990).
[23]J. Li, C.-G. Duan, Z.-Q. Gu, D.-S. Wang, Phys. Rev. B **57**, 6925 (1998).
[24]Z. Lin, J. Lin, Z. Wang, C. Chen, M.-H. Lee, Phys. Rev. B **62**, 1757 (2000).
[25]Z. S. Lin, J. Lin, Z. Z. Wang, Y. C. Wu, N. Ye, C. T. Chen, and R. K. Li, J. Phys. Cond. Matter **13**, R369 (2001).
[26]Y. Noel, M. Catti, and R. Dovesi, Ferroelectrics **300**, 139 (2004).
[27]D. Vanderbilt, J. Phys. Chem. Solids **61**, 147 (2000).
[28]R. Resta, D. Vanderbilt, in *Physics of Ferroelectrics: A Modern Perspective* (edited by K. M. Rabe, C. H. Ahn, and J.-M. Triscone (Springer-Verlag, Berlin, 2007).
[29]M. Costache, I. Mateia, L. Pintiliea, H. V. Alexandrua, and C. Berbecaru, J. Optoelectron. Adv. Mater. **3**, 75 (2001).
[30]W. Martienssen and H. Warlimont, editors, *Springer Handbook of Condensed Matter and Materials Data* (Springer, Berlin, 2005).
[31]J. Q. Yao, W. Sheng, and W. Shi, J. Opt. Soc. Am. B. **9**, 891 (1992).
[32]D.-S. Wang, Bull. Mater. Sci. **26**, 159 (2003).
[33]B. Wu, N. Chen, and C. Chen, Opt. Lett. **14**, 1080 (1989).
[34]M. Ebrahimzadel, G. Robertson, and M. H. Dunn, Opt. Lett. **16**, 767 (1991).
[35]C. D. Gribble and A. J. Hall, *Optical Mineralogy* (Routledge, London, 2003).
[36]M. Yamazaki and T. Ogawa, J. Opt. Soc. Am. **54**, 1215 (1964).
[37]T. Ozaki, K. Furuta, M. Ninomiya, Y. Yamazaki, T. Yoshida, and E. Nakamura, J. Phys. Soc. Jpn. **59**, 2251 (1990).
[38]S. Saito and R. Onaka, Ferroelectrics **21**, 553 (1978).
[39]R. Orlando, V. Lacivita, R. Bast, and K. Ruud, J. Chem. Phys. **132**, 244106 (2010).
[40]H. Ito, H. Naito, and H. J. Inaba, Appl. Phys. **46**, 3992 (1975).
[41]R. W. Boyd, *Nonlinear Optics* (Academic Press, San Diego, CA, 2003).
[42]M. E. Lines and A. M. Glass, *Principles and Application of Ferroelectrics and Related Materials* (Clarendon Press, Oxford, 1977).
[43]S. Sharma and C. Ambrosch-Draxl, Phys. Scr. **T109**, 128 (2004).
[44]B. Adolph and F. Bechstedt, Phys. Rev. B **62**, 1706 (2000).
[45]C.-G. Duan, J. Li, Z.-Q. Gu, and D.-S. Wang, Phys. Rev. B **60**, 9435 (1999).
[46]*Landolt-Börnstein: Numerical Data and Functional Relationship in Science and Technology*, New Series, Group III, edited by K.-H. Hellwege, Vol. 16 (Springer, Berlin, 1984).
[47]J. Q. Yao and T. S. Fahlen, J. Appl. Phys. **55**, 65 (1984).
[48]S. K. Kurtz and T. T. Perry, J. Appl. Phys. **39**, 87 (1968).